nature structural & molecular biology

Electron microscopy structure of human APC/C^{CDH1}–EMI1 reveals multimodal mechanism of E3 ligase shutdown

Jeremiah J Frye[1,8], Nicholas G Brown[1,8], Georg Petzold[2,8], Edmond R Watson[1,3], Christy R R Grace[1], Amanda Nourse[4], Marc A Jarvis[2], Richard W Kriwacki[1,3], Jan-Michael Peters[2], Holger Stark[5,6] & Brenda A Schulman[1,3,7]

The anaphase-promoting complex/cyclosome (APC/C) is a ~1.5-MDa multiprotein E3 ligase enzyme that regulates cell division by promoting timely ubiquitin-mediated proteolysis of key cell-cycle regulatory proteins. Inhibition of human APC/C^{CDH1} during interphase by early mitotic inhibitor 1 (EMI1) is essential for accurate coordination of DNA synthesis and mitosis. Here, we report a hybrid structural approach involving NMR, electron microscopy and enzymology, which reveal that EMI1's 143-residue C-terminal domain inhibits multiple APC/C^{CDH1} functions. The intrinsically disordered D-box, linker and tail elements, together with a structured zinc-binding domain, bind distinct regions of APC/C^{CDH1} to synergistically both block the substrate-binding site and inhibit ubiquitin-chain elongation. The functional importance of intrinsic structural disorder is explained by enabling a small inhibitory domain to bind multiple sites to shut down various functions of a 'molecular machine' nearly 100 times its size.

Ubiquitin (Ub) ligation by the action of E1-E2-E3 enzyme cascades is a widespread mechanism that controls protein function. After E1-mediated formation of a transient, thioester-bonded E2~Ub intermediate, E3s promote Ub ligation to specific protein substrates ("~" denotes covalent complex; "–", noncovalent complex). The 600 predicted members of the largest human E3 family contain a RING domain that binds and activates an E2~Ub intermediate to ligate Ub to a substrate recruited to a distal protein-interaction domain[1]. APC/C is a behemoth ~1.5 MDa E3 that controls cell division by promoting timely Ub-mediated proteolysis of key regulatory proteins. Human APC/C has at least 14 core subunits (APC1, APC2, APC3 (CDC27), APC4, APC5, APC6 (CDC16), APC7, APC8 (CDC23), APC10 (DOC1), APC11, APC13, APC15, APC16 and CDC26), several of which are present in duplicate in each holo APC/C enzyme[2,3]. APC/C is activated at different stages of the mitotic cell cycle by association with either CDC20 or CDH1, which target proteins for ubiquitination by binding substrate KEN-box motifs directly and recruiting substrate D-box sequences in collaboration with APC10 (refs. 4–7). To prevent chromosome segregation defects such as aneuploidy, CDC20 assembles with MAD2, MAD3 (BUBR1) and BUB3 to form a mitotic checkpoint complex (MCC) that binds and inhibits APC/C until all chromosomes are properly bioriented on the mitotic spindle[8,9]. MCC serves as a decoy KEN-box–based substrate–receptor complex, which blocks APC/C association with free CDC20 and bona fide KEN- and D-box–containing substrates[5,10].

Following MCC disassembly, APC/C associates with free CDC20 to promote Ub-mediated proteolysis of substrates such as cyclin B and securin to initiate chromosome segregation. Subsequently, APC/C associates with CDH1 to regulate exit from mitosis and during G1 to promote Ub-mediated turnover of regulators of the G1-S transition and DNA replication. In higher eukaryotes, APC/C^{CDH1} is restrained during interphase by the distinctive EMI1 (Rca1 in *Drosophila*)[11–14]. APC/C inhibition by EMI1 allows accumulation of substrates such as mitotic cyclins and geminin[11,15–17]. EMI1 also functions later in a localized manner, inhibiting APC/C^{CDH1}-mediated ubiquitination of cyclin B at spindle poles[18]. Misregulation of EMI1 leads to endoreduplication and mitotic defects such as abnormal spindles and excess centrosomes[14,16,17,19,20].

EMI1 has three domains. The N-terminal domain mediates regulatory interactions that control localization and EMI1's own stability[18,21]. An F-box binds SKP1 but to date has not been shown to function in APC/C inhibition[12,19]. The C-terminal domain is responsible for APC/C inhibition and contains a D-box, linker sequence, a zinc-binding region (ZBR) and a C-terminal tail[12,22]. Previous reports concluded that the EMI1 C-terminal domain is a pseudosubstrate inhibitor that binds to CDH1 and competes in a D-box– and ZBR-dependent manner with the substrate cyclin B for binding to APC/C^{CDH1} (refs. 12,22). However, studies of the homologous meiotic APC/C inhibitor EMI2 suggested that a key inhibitory region is the C-terminal tail[23,24]. Despite its importance, structural mechanisms by which EMI1 inhibits APC/C^{CDH1} are unknown.

[1]Department of Structural Biology, St. Jude Children's Research Hospital, Memphis, Tennessee. [2]Research Institute of Molecular Pathology, Vienna, Austria. [3]Department of Microbiology, Immunology and Biochemistry, University of Tennessee Health Sciences Center, Memphis, Tennessee. [4]Hartwell Center for Bioinformatics and Biotechnology, St. Jude Children's Research Hospital, Memphis, Tennessee. [5]Max Planck Institute for Biophysical Chemistry, Göttingen, Germany. [6]Department of 3D Electron Cryomicroscopy, Institute of Microbiology and Genetics, Georg-August Universität, Göttingen, Germany. [7]Howard Hughes Medical Institute, St. Jude Children's Research Hospital, Memphis, Tennessee. [8]These authors contributed equally to this work. Correspondence should be addressed to J.-M.P. (jan-michael.peters@imp.ac.at), H.S. (hstark1@gwdg.de) or B.A.S. (brenda.schulman@stjude.org).

Received 4 January; accepted 9 April; published online 26 May 2013; doi:10.1038/nsmb.2593

To understand EMI1-mediated inhibition of APC/C, we performed a hybrid structural analysis. NMR studies indicated that other than the 45-residue ZBR, the 143-residue C-terminal EMI1 inhibitory region lacks fixed tertiary structure. Electron microscopy (EM) studies revealed that EMI1 interacts with, approaches and/or alters the conformations of numerous subunits of the ~1.5 MDa APC/C^{CDH1} molecular machine. The functional importance of intrinsic structural disorder is explained by the D-box, linker, ZBR and tail synergistically blocking both Ub ligation to a substrate and Ub-chain elongation by APC/C.

RESULTS

Structural dissection of EMI1's APC/C inhibitory domain

To guide structural studies, we analyzed the human EMI1 protein sequence with the program PONDR (http://www.pondr.com/index) to identify folded domains[25]. The majority of EMI1 is predicted to be intrinsically disordered, with the exception of a short N-terminal region, the F-box and the ZBR (**Fig. 1a**). In the APC/C-inhibitory C-terminal domain, regions predicted to be unstructured include the D-box, linker region and tail. To test this hypothesis, we characterized structural properties for the EMI1 C-terminal domain (hereafter referred to as EMI1^{DLZT} for D-box, linker, ZBR, tail) by NMR. Backbone resonance assignments revealed that the chemical shifts were consistently dispersed for the ZBR residues in the EMI1^{DLZT}, EMI1^{ZT} and EMI1^{Z} constructs, indicating that the ZBR is an autonomously folded domain (**Fig. 1b**). Notably, the remaining resonances in EMI1^{DLZT} displayed poor dispersion, low or negative {^{1}H}-^{15}N heteronuclear NOE (HetNOE) values and relatively low differences in Cα chemical shifts compared with values predicted for a random coil (**Fig. 1c**).

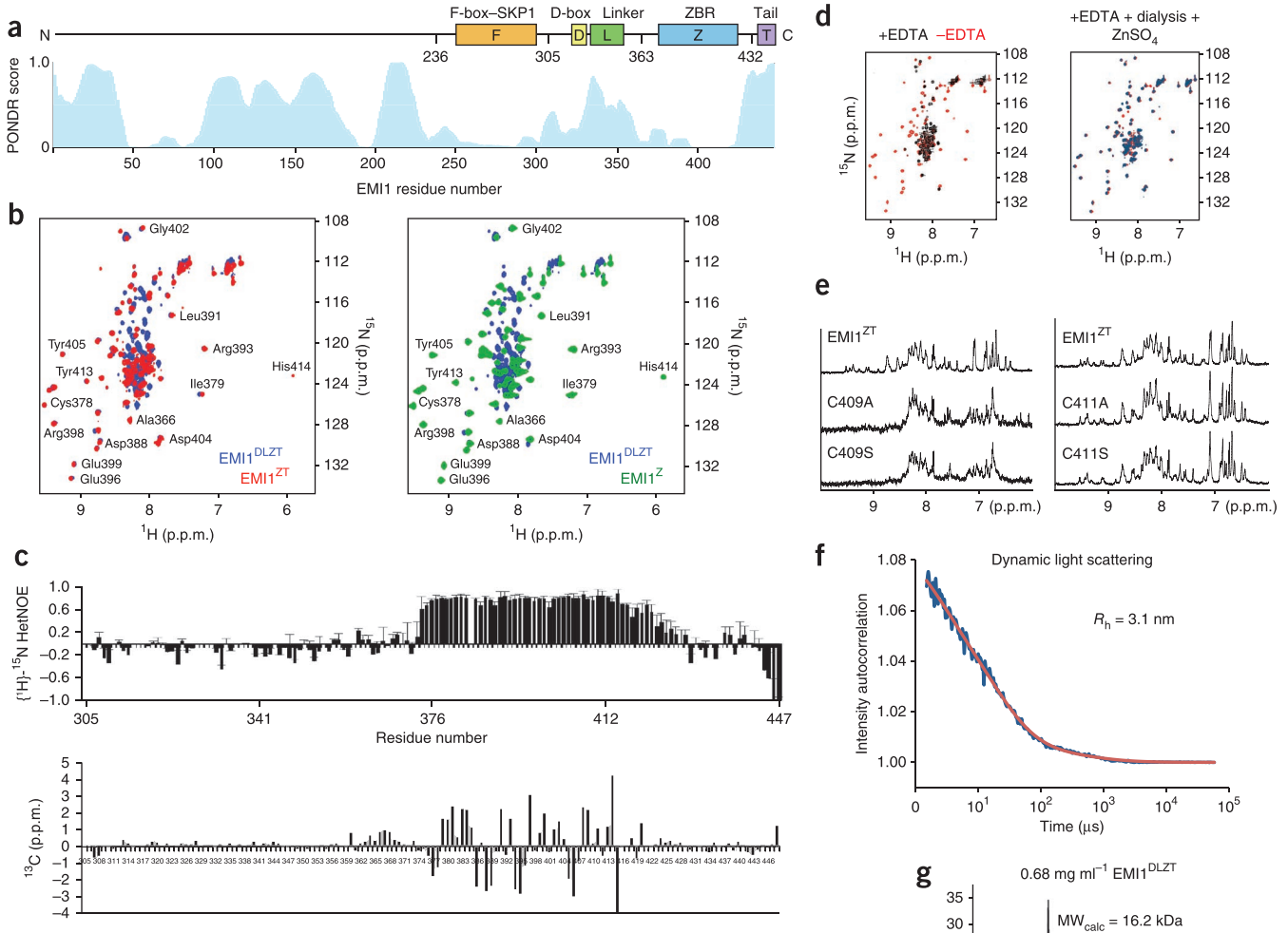

Figure 1 The APC/C inhibitory domain of EMI1 contains two intrinsically disordered segments separated by a zinc-dependent folded domain. (**a**) Output of structure prediction program PONDR, with schematic views of EMI1 structural elements shown above. F, F-box–SKP1; D, D-box; L, linker; Z, zinc-binding region; T, tail. (**b**) Overlay of ^{15}N-^{1}H HSQC spectra of uniformly ^{15}N-labeled EMI1^{DLZT} (blue, consisting of the DLZT, corresponding to the APC/C^{CDH1} inhibitory domain[12,22]), with EMI1^{ZT} (red) or EMI1^{Z} (green) superimposition showing dispersal of peaks found in the isolated EMI1^{Z} domain. A subset of disperse resonances assigned for EMI1^{DLZT} are labeled. (**c**) Heteronuclear NOE data and difference in Cα chemical shifts (measured value to predicted value for random coil[50]) for uniformly ^{15}N-labeled EMI1^{DLZT} measured at 25 °C. Similar results obtained at 5 °C are not shown. (**d**) Overlay of ^{15}N-^{1}H HSQC spectrum of EMI1^{ZT} (red) with that after treatment with EDTA (black) on left and after subsequent reconstitution with zinc (blue) on right. (**e**) One-dimensional proton NMR spectra for EMI1^{ZT} or the indicated cysteine mutants. (**f**) Dynamic light scattering data (DynaPro Nanostar) and fit for hydrodynamic radius (Dynamics V7.1.7 software, Wyatt) for EMI1^{DLZT}. (**g**) Analytical ultracentrifugation data showing sedimentation coefficient distribution (c(*s*)) analysis for determination of sedimentation coefficient for EMI1^{DLZT}, for calculation of hydrodynamic radius.

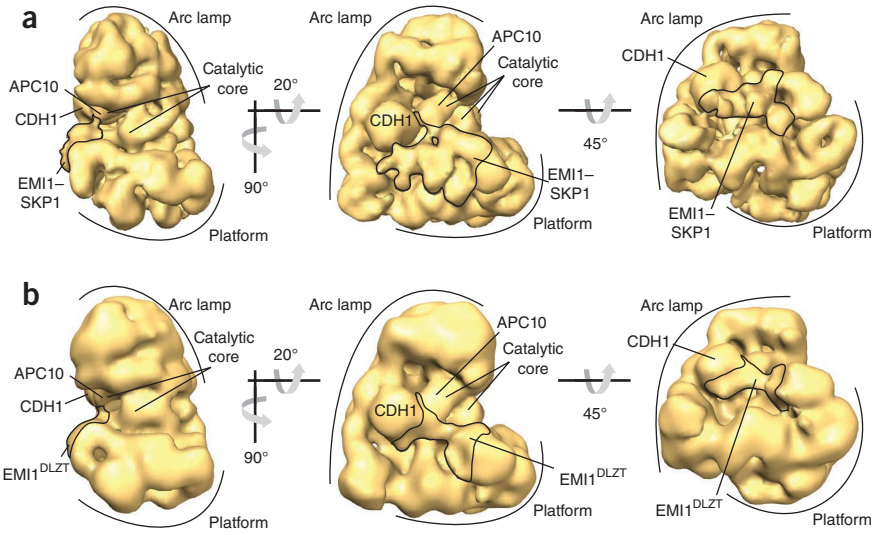

Figure 2 EM structures of APC/C^{CDH1} inhibited by EMI1–SKP1 and the inhibitory C-terminal domain (EMI1^{DLZT}). (**a**) Three views of human APC/C^{CDH1}–EMI1–SKP1, showing the structural superdomains of APC/C (arc lamp, platform and catalytic core) and the CDH1 and APC10 D-box co-receptors. The density attributed to EMI1–SKP1 is outlined. (**b**) Three views of human APC/C^{CDH1}–EMI1^{DLZT}, showing the structural superdomains of APC/C (arc lamp, platform and catalytic core) and the CDH1 and APC10 D-box co-receptors. The density attributed to EMI1^{DLZT} is outlined.

Previous studies showed that mutation of ZBR cysteines or treatment with a metal chelator decreased EMI1's competition with substrate binding or inhibition of substrate ubiquitination by APC/C[19,22]. We found that the addition of a metal chelator, EDTA, to ^{15}N-labeled EMI1^{ZT} eliminated the ^{15}N-^{1}H chemical shift dispersion that is characteristic of the folded structure, which was re-established by $ZnSO_4$ addition (**Fig. 1d**). To resolve the ambiguity of one potential zinc-coordinating residue[19], we ascertained that mutation of Cys409, but not Cys411, eliminated the hallmarks of folding in one-dimensional proton NMR spectra (**Fig. 1e**).

To further characterize the biophysical properties of EMI1^{DLZT}, we measured the hydrodynamic radius (R_h) to be 3.1 nm and 2.9 nm by dynamic light scattering (DLS) and analytical ultracentrifugation, respectively (**Fig. 1f,g**). A globular protein would have to be ~46 kDa, rather than the 16.0 kDa of EMI1^{DLZT}, to yield an R_h value of 3.1 nm by DLS. The best-fit, weight-average anhydrous frictional ratio $(f/f_0)_w$ values of 1.73 and 1.85 obtained from two analytical ultracentrifugation experiments indicate that EMI1^{DLZT} is elongated in solution (**Supplementary Fig. 1**). Overall, the data suggest that EMI1^{DLZT} is substantially intrinsically unfolded, with predominantly disordered D-box, linker and tail regions separated by a folded ZBR.

EM reveals multisite EMI1 binding to APC/C^{CDH1}

Previous EM studies revealed a structurally dynamic triangular APC/C architecture organized from three superdomains: (i) an 'arc lamp' comprising TPR subunits APC7, APC3, APC6 and APC8 and associated small subunits APC16, APC13 and CDC26; (ii) a 'platform' comprising APC1, APC4, APC5 and APC15; and (iii) a catalytic core, located between the arc lamp and platform, containing the APC2-APC11 cullin–RING complex and the substrate co-receptor, APC10 (ref. 6,10). These superdomains surround a large central cavity containing the substrate-binding site and proposed catalytic site[26]. Different conformers were observed for apo-APC/C, which vary in relative positions for the arc lamp and platform, reflecting the dynamic nature of the complex[10]. CDH1 binds APC3 in the arc lamp, with its substrate-binding WD40 domain projecting toward the catalytic core[27].

To understand the structural basis for inhibition, we performed a series of single-particle reconstructions by negative-stain EM on complexes between APC/C purified from HeLa cells reconstituted with CDH1 and various versions of EMI1. Versions of EMI1 containing an F-box were complexed with SKP1. In comparison to human APC/C^{CDH1} (ref. 6), the APC/C^{CDH1}–EMI1–SKP1 complex displays additional prominent density, which we attribute to EMI1–SKP1 (**Fig. 2a** and **Supplementary Fig. 2a,b**). EMI1–SKP1 occupies and thus occludes access to the entire central cavity of APC/C. One edge of EMI1–SKP1 approaches the base of the arc lamp and the CDH1 WD40 domain. The other side is contiguous and integrated with the platform.

EM analysis further reveals that despite its small size, the inhibitory domain, EMI1^{DLZT}, retains key features to obstruct APC/C^{CDH1}

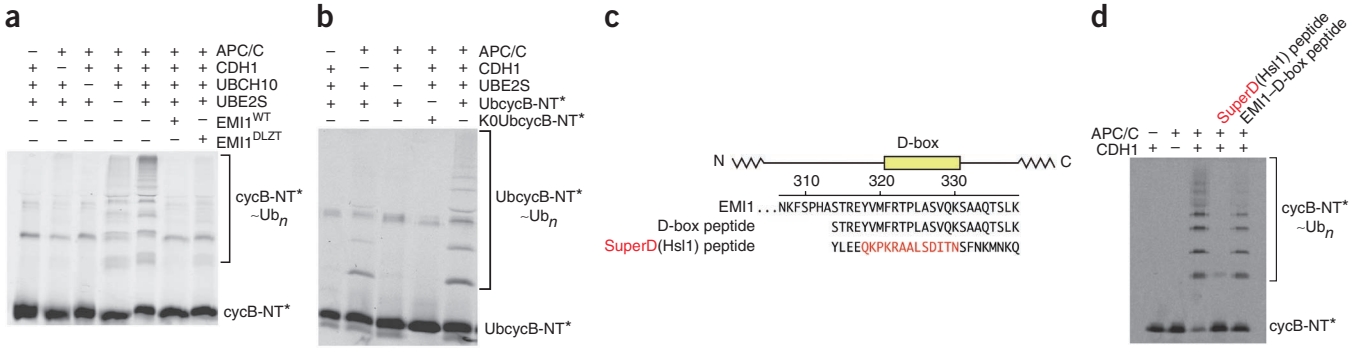

Figure 3 EMI1 is a tight binding inhibitor of APC/C Ub ligation and Ub-chain formation. (**a**) Fluorescence detection of cycB-NT* ubiquitination by APC/C^{CDH1} with UBCH10, alone or in combination with UBE2S, in the absence or presence of EMI1–SKP1 or EMI1^{DLZT}. (**b**) Fluorescence detection of APC/C-dependent UbcycB-NT* ubiquitination by UBE2S in the absence of UBCH10 and in the absence or presence of CDH1. The K0UbcycB-NT* substrate has all lysines in the Ub moiety mutated to arginines. (**c**) Sequence alignment of the EMI1 D-box region with EMI1 and Hsl1 D-box peptides. (**d**) Fluorescence detection of cycB-NT* ubiquitination by APC/C^{CDH1} and UBCH10 in the absence or presence of the indicated D-box peptides at 100 μM.

activity (**Fig. 2b** and **Supplementary Fig. 2c**). For the complexes with both EMI1–SKP1 and EMI1^{DLZT}, there are differences in the vicinity of the D-box co-receptors CDH1 and APC10 and additional density linking this region and the catalytic core and platform regions. Substantial additional density is also observed emanating from the platform. Notably, relative to prior apo-APC/C and APC/C^{CDH1} structures, in both EMI1-inhibited complexes the catalytic core forms a prominent contact with platform regions assigned to APC1 and APC4, which are repositioned. The density assigned to APC1 and APC4 has lost contact with APC5, is no longer in the position previously observed for apo-APC/C[26,27] and is instead bent toward the catalytic core.

Table 1 Apparent K_i values for EMI1 variants in the indicated APC/C-dependent ubiquitination reactions

E2 substrate	UBCH10 cycB-NT*	UBCH10 UbcycB-NT*	UBE2S UbcycB-NT*	No CDH1, UBE2S UbcycB-NT*	No CDH1, UBE2S Ub*
	K_i app (nM)	K_i app (nM)	K_i app (nM)	K_i app (nM)	K_i app (nM)
EMI1–SKP1	≤2.5	≤2.5	≤2.5	690 ± 130	230 ± 35
EMI1^{FDLZT}	≤2.5	≤2.5	≤2.5	NT	NT
EMI1^{DLZT}	≤2.5	≤2.5	≤2.5	NT	NT
EMI1$^{D(Mut)LZT}$	>10,000	>10,000	810 ± 230	NT	220 ± 37
EMI1^{NFDLZ}	440 ± 60	360 ± 47	940 ± 220	NT	>6,000
EMI1^{NFDL}	510 ± 120	330 ± 74	1,500 ± 340	NT	NT
EMI1^{ZT}	>10,000	>10,000	520 ± 86	NT	2,000 ± 400
EMI1^{Z}	>80,000	>80,000	>80,000	NT	>80,000
EMI1^{T}	>1 mM[a]	>1 mM[a]	42,000 ± 12,000	48,000 ± 12,000	13,000 ± 2,400

[a]≥5 mM peptide changes pH. NT, not tested.

A difference map comparing the full APC/C^{CDH1}–EMI1–SKP1 complex with APC/C^{CDH1}–EMI1^{DLZT} reveals additional exposed density more distal from the APC/C central cavity and catalytic core, which we attribute to the N-terminal domain and SKP1-bound F-box (**Supplementary Fig. 2d**). This agrees with the location of extra density for a complex harboring a maltose-binding protein fused at the N terminus of SKP1 (**Supplementary Fig. 2e**).

Tight-binding inhibition of substrate ubiquitination

APC/C^{CDH1} utilizes a two-step mechanism to mediate substrate polyubiquitination[28]. First, APC11 activates Ub transfer from an E2 (often UBCH10 in human cells) directly to the substrate[29–32]. Second, another E2 (UBE2S in humans[32–35]) transfers Ub to a substrate-ligated Ub to mediate chain elongation[28,36].

Because of the large quantities of APC/C required to dissect mechanisms underlying EMI1-mediated inhibition, we turned to a recombinant APC/C system[37]. The hallmark features of endogenous human APC/C were recapitulated in our assays using a fluorescently tagged cyclin B N-terminal domain (cycB-NT*) as the substrate: ubiquitination depends on APC/C and CDH1, with low-molecular-weight products being formed by UBCH10, high-molecular-weight (HMW) products being formed by UBCH10 and UBE2S together, and inhibition being produced by EMI1–SKP1 and EMI1^{DLZT} (**Fig. 3a**). This prompted us to develop assays to separately investigate APC/C-mediated ubiquitination with the two E2s. We were able to quantify APC/C^{CDH1}–UBCH10–mediated ubiquitination of both cycB-NT* and a fluorescent Ub fusion (UbcycB-NT*), which is also a substrate for APC/C^{CDH1}–UBE2S–mediated ubiquitination even in the absence of UBCH10 (**Fig. 3b**).

We first performed a series of titrations to determine the saturating concentrations of CDH1 and identify conditions in which the ubiquitination reactions were in initial rate regimes (**Supplementary Figs. 3–5**). Subsequent titrations of UBCH10, UBE2S and substrate allowed measurement of K_m values (**Supplementary Fig. 3d**). The K_m of 290 ± 80 nM for cycB-NT* in reactions with UBCH10 closely agrees

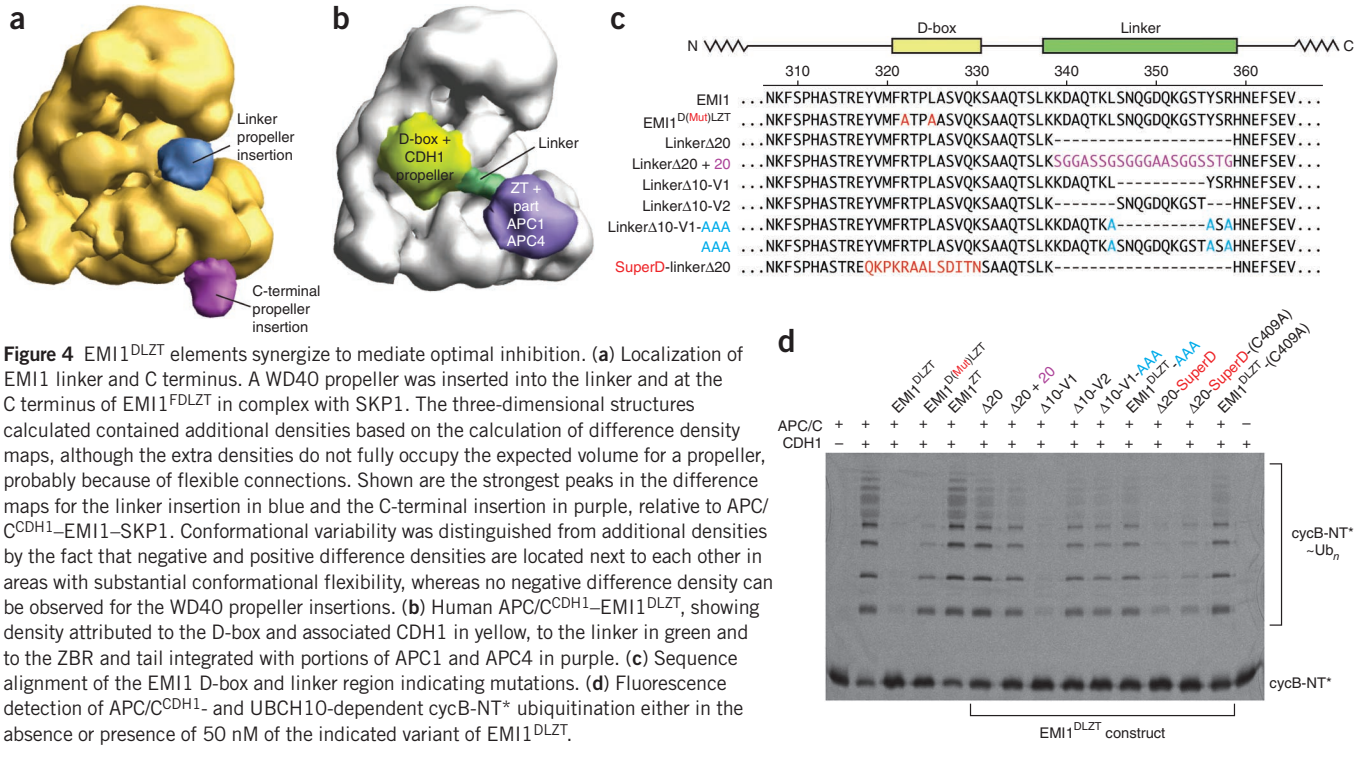

Figure 4 EMI1^{DLZT} elements synergize to mediate optimal inhibition. (**a**) Localization of EMI1 linker and C terminus. A WD40 propeller was inserted into the linker and at the C terminus of EMI1^{FDLZT} in complex with SKP1. The three-dimensional structures calculated contained additional densities based on the calculation of difference density maps, although the extra densities do not fully occupy the expected volume for a propeller, probably because of flexible connections. Shown are the strongest peaks in the difference maps for the linker insertion in blue and the C-terminal insertion in purple, relative to APC/C^{CDH1}–EMI1–SKP1. Conformational variability was distinguished from additional densities by the fact that negative and positive difference densities are located next to each other in areas with substantial conformational flexibility, whereas no negative difference density can be observed for the WD40 propeller insertions. (**b**) Human APC/C^{CDH1}–EMI1^{DLZT}, showing density attributed to the D-box and associated CDH1 in yellow, to the linker in green and to the ZBR and tail integrated with portions of APC1 and APC4 in purple. (**c**) Sequence alignment of the EMI1 D-box and linker region indicating mutations. (**d**) Fluorescence detection of APC/C^{CDH1}- and UBCH10-dependent cycB-NT* ubiquitination either in the absence or presence of 50 nM of the indicated variant of EMI1^{DLZT}.

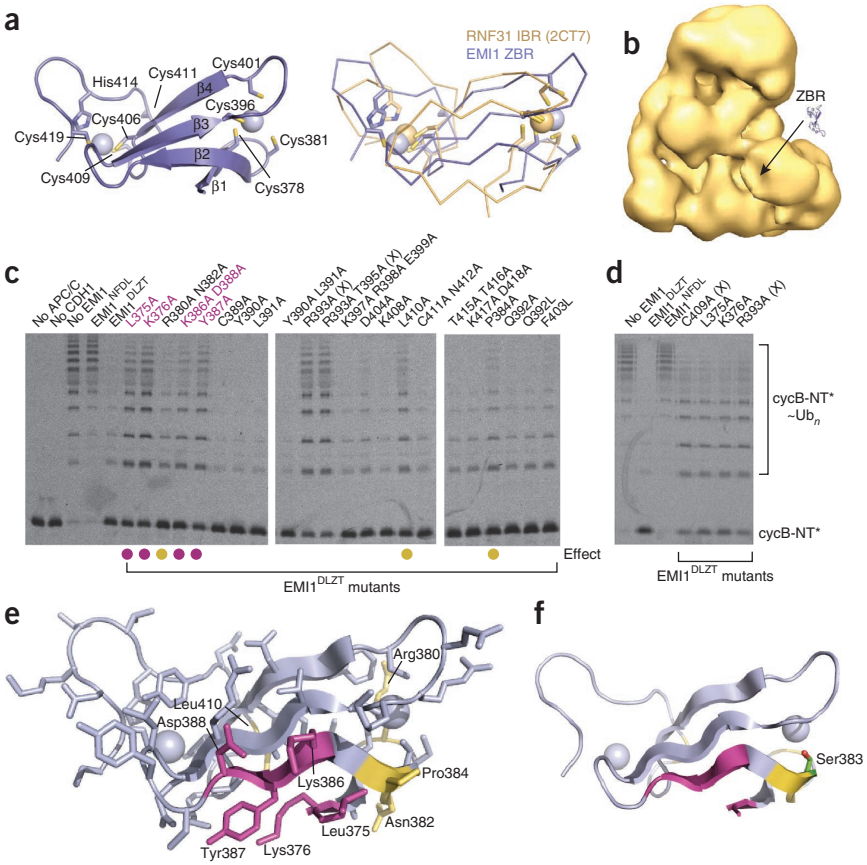

Figure 5 NMR structure of the ZBR and identification of a surface required for inhibition. (**a**) Solution structure of the ZBR portion of EMI1^{ZT} as cartoon with zincs as spheres on left, and as ribbons superimposed with the RNF31 (PDB 2CT7, gold) IBR on right. (**b**) The crystal structure of the EMI1 ZBR is shown with approximate location next to the EM structure of APC/C^{CDH1}–EMI1^{DLZT} at the same scale. (**c**) Alanine scan testing roles of indicated ZBR side chains on EMI1^{DZLT}-mediated inhibition of cycB-NT* ubiquitination by APC/C^{CDH1} and UBCH10. Inhibition by wild-type EMI1^{DLZT} and EMI1^{NFDL}–SKP1 (lacking the ZBR and tail) are shown for comparison. (X) denotes unfolded mutants. Mutants displaying the greatest decrease in inhibitory activity are marked with purple dots; those with a lesser decrease in inhibitory activity are marked with gold dots. (**d**) Comparison of the effects of the indicated surface alanine mutants and the unfolding C409A mutant on EMI1^{DZLT}-mediated inhibition of cycB-NT* ubiquitination by APC/C^{CDH1} and UBCH10. (**e**) Structure of EMI1 ZBR showing all side chains mutated in alanine scan as sticks, with those causing the greatest decrease in inhibitory activity in purple and a lesser decrease in inhibitory activity in gold. (**f**) Location of Ser383 (side chain shown as green stick with oxygen in red) cyclin-dependent kinase–mediated phosphorylation site on cartoon representation of EMI^{ZT} structure with the two zinc atoms shown as spheres, the sites of Ala mutations that impair EMI1^{DLZT}-mediated inhibition colored as in panel **e**. Ser383 is among three cyclin-dependent kinase sites that when phosphorylated impair EMI1 inhibition of APC/C[49].

with previous measurements of 228 and 63 nM for similar substrates with immunopurified endogenous *Xenopus laevis* and *Saccharomyces cerevisiae* APC/C, respectively[38,39].

Experiments with EMI1–SKP1 revealed tight binding inhibition, which we quantified using the Morrison equation[40]. Performing experiments under initial rate conditions required our use of 5 nM APC/C^{CDH1}, for which the tight binding nature of EMI1 and data quality at the stoichiometric point (1:1 APC/C^{CDH1}:EMI1) restricted our accurate quantification of apparent K_i (K_i^{app}) values to a lower limit of 2.5 nM (**Supplementary Fig. 5d**). Titration of EMI1–SKP1 revealed K_i^{app} values of ≤2.5 nM, and potentially substantially lower, for APC/C^{CDH1}-mediated substrate ubiquitination with both UBCH10 and UBE2S, as approximately 5 nM of EMI1–SKP1 completely inhibits these reactions (**Table 1**). Similar results were obtained for a version lacking the EMI1 N terminus or the entire N-terminal domain and F-box–SKP1, which consisted exclusively of the C-terminal D-box, linker, ZBR and tail regions. Below we describe how the distinct elements within EMI1^{DLZT} contribute to a tight binding mode of APC/C^{CDH1} inhibition.

EMI1 has an essential but relatively weak D-box

An obvious key functional element is EMI1's D-box. In examining the EM data, there were differences between APC/C^{CDH1} and the EMI1–SKP1– and EMI1^{DLZT}-bound complexes in the vicinity of CDH1 and APC10, consistent with EMI1's D-box binding the co-receptors (**Supplementary Fig. 2**). We were unable to generate stoichiometric complexes for mutants lacking EMI1's D-box. Furthermore, alanine substitutions in place of Arg322 and Leu325 in EMI1^{DLZT}'s D-box RxxL motif decreased inhibition of cycB-NT* in reactions with UBCH10 to the point that we could not measure a K_i under the initial rate conditions (**Table 1**). The K_i^{app} increased by over two orders of magnitude for UbcycB-NT* ubiquitination by APC/C^{CDH1} and UBE2S.

Despite its requirement, the EMI1 D-box on its own is relatively weak: an isolated EMI1^{D} peptide is insufficient as an inhibitor even at the 100 μM concentration we could achieve in our assays. This contrasts with an isolated D-box peptide from the *S. cerevisiae* APC/C substrate Hsl1 (ref. 41), which is a more potent inhibitor (**Fig. 3c**,**d**).

EMI1 elements synergize to inhibit substrate ubiquitination

In order to map the locations of the remaining portions of EMI1, we generated single-particle EM reconstructions for mutants in EMI1^{FDLZT}–SKP1 with insertions between residues 354 and 355 in the linker upstream of the ZBR and at the C terminus of EMI1 (**Fig. 4a**). In this latter case, it was necessary to replace the EMI1 D-box with that from Hsl1 to enhance complex formation. The insertions contained the β-propeller from *S. cerevisiae* Doa1, which has N and C termini in close proximity[42]. Although we cannot be certain that the insertions do not alter native interactions, the data are consistent with the linker projecting away from the D-box bound to CDH1 and APC10 and toward the APC/C platform and catalytic core and with the ZBR and tail extending across the platform (**Fig. 4a**,**b**).

Prompted by the structural data showing that an insertion maps to the central location between the D-box co-receptor APC10, the

arc lamp and the platform (**Fig. 4a**), we considered that the linker might be functionally important. Indeed, the linker is not simply a spatial connector joining the D-box and ZBR effectors: deleting 20 linker residues impairs EMI1^{DLZT}-mediated inhibition, which is not restored by replacing them with a 20-residue, glycine-rich sequence (**Fig. 4c**,**d**). As a first attempt to address whether this sequence or structure may be important, we tested two 10-residue deletions and found only one to cause severely impaired inhibition. Triply mutating conserved Leu345, Tyr356 and Arg358 within the essential sequence to alanines, either in the context of the benign 10-residue deletion or in EMI1^{DLZT}, was sufficient to substantially impair inhibition. Thus, specific side chains within the linker contribute to inhibition (**Fig. 4d**).

One reason the linker or other C-terminal elements may be important would be to compensate for EMI1's relatively weak D-box. Inhibitory roles of regions other than the D-box are reflected by the D-box–mutated version of EMI1$^{D(Mut)LZT}$ inhibiting formation of HMW conjugates after extended reaction times with UBCH10 despite causing no measurable inhibition under initial rate conditions (**Fig. 4d**, **Table 1** and **Supplementary Fig. 6**). In contrast, grafting the Hsl1 'Super'D-box into EMI1^{DLZT} largely overcame the defects resulting from deleting the linker, even in combination with the ZBR-unfolding C409A mutation (**Fig. 4d**). Thus, it appears that EMI1's weak but essential D-box must function combinatorially with additional elements for optimal inhibition. C-terminal deletions, which retained the D-box and linker (EMI1^{FDLZ} and EMI1^{FDL}) but lacked the tail or both the ZBR and tail, inhibited the reactions with both E2-substrate pairs, with K_i^{app} values increased by more than two orders of magnitude. Notably, deleting the ZBR had little effect in the absence of the EMI1 C-terminal tail; this underscores the importance of the tail in functioning with the D-box and/or linker to maximally inhibit APC/C^{CDH1} activity with both E2s (**Table 1**). Taken together, the data suggest that the D-box, linker, ZBR and tail bind multiple sites on APC/C^{CDH1} to synergistically antagonize ubiquitination activity.

NMR structure and inhibitory surface of the EMI1 ZBR

To gain insights into potential contributions of the ZBR in APC/C inhibition, we assigned backbone and side-chain resonances of ^{13}C, ^{15}N-labeled EMI1^{ZT} and determined the solution structure (**Fig. 5a**,**b** and **Table 2**). Although the EMI1^{ZT} construct spans residues 363–447, only residues 375–420 exhibited the features of a folded domain, with a central, twisted, four-stranded β-sheet and two zinc ions on opposite ends of the sheet. One zinc is chelated by the β1-β2 and β3-β4 loops, and the other by the β2-β3 loop and a loop following β4. The ZBR displays an In-Between-RING (IBR) domain topology, aligning with the IBR of RNF31 with 5.5 Å r.m.s. deviation.

The NMR structure enabled identification of a functionally important surface on the ZBR through alanine-scanning mutagenesis of EMI1^{DLZT}. Under conditions in which APC/C^{CDH1} is insensitive to a version of EMI1 lacking the ZBR and tail (EMI1^{NFDL}) but is inhibited by wild-type EMI1^{DLZT}, several mutants impaired EMI1^{DLZT}-mediated inhibition of APC/C^{CDH1} ubiquitination with either UBCH10 or UBE2S (not shown) (**Fig. 5c**,**d**). The majority of defective mutants (L375A, K376A, R380A N382A, K386 D388A, Y387A, P384A) mapped to a single surface (**Fig. 5e**,**f**). The diminished inhibition caused by the three most deleterious individual alanine mutants—at positions Leu375, Lys376 and Arg393—resembled that caused by unfolding the ZBR through mutation of the Cys409 zinc ligand (**Fig. 5d**). Although we found the R393A mutant to also be unfolded, NMR analysis of ^{15}N-labeled samples confirmed folding of the L375A and K376A mutants (**Supplementary Fig. 7**), suggesting that the ZBR is not solely a structured tether between the linker and tail. Rather, the surface harboring these residues is important for inhibition. Leu375 and Lys376 are at the N terminus of the ZBR domain, suggesting spatial proximity between the inhibitory ZBR surface and the upstream linker sequence in EMI1.

Table 2 NMR and refinement statistics

	Protein
NMR distance and dihedral constraints	
Distance constraints	
Total NOE	931
Intra-residue	381
Inter-residue	
Sequential ($\|i-j\|=1$)	211
Medium range ($\|i-j\|<4$)	83
Long range ($\|i-j\|>5$)	256
Intermolecular	8
Hydrogen bonds	32
Total dihedral angle restraints	
ϕ	19
ψ	19
Structure statistics	
Violations (mean ± s.d.)	
Distance constraints (Å)	0.0093 ± 0.001
Dihedral angle constraints (°)	0.1833 ± 0.061
Max. dihedral angle violation (°)	0.8600 ± 0.300
Max. distance constraint violation (Å)	0.2100 ± 0.060
Deviations from idealized geometry	
Bond lengths (Å)	0.0
Bond angles (°)	0.0
Impropers (°)	0.015
Average pairwise r.m.s. deviation (Å)[a]	
Heavy	0.554
Backbone	0.954

[a]Backbone and heavy atom r.m.s. deviations were calculated by superimposing residues 375–420 of the 20 lowest-energy conformers of EMI1^{ZT}.

ZBR and C-terminal tail synergize to block chain elongation

A distinctive pattern of inhibition was observed for the EMI1 fragment consisting only of the ZBR and tail, which on its own inhibited APC/C^{CDH1}–UBE2S–mediated ubiquitination of UbcycB-NT*, although relatively weakly, with a K_i^{app} of 520 nM (**Table 1**). The ZBR and tail synergize, as we could not measure inhibition with the isolated ZBR at the highest concentration we could achieve, and the K_i^{app} increased to 42 μM for a synthetic peptide corresponding to the isolated EMI1^{T}. We did not observe obvious effects of EMI1^{ZT} on the initial rate of Ub ligation by UBCH10 (**Table 1**).

Because the EM data indicated that the EMI1^{ZT} region interacts with the APC/C catalytic core and/or platform regions (**Fig. 4a**), we tested whether EMI1^{ZT} inhibits APC/C^{CDH1}–UBE2S–mediated Ub ligation independently of counteracting substrates recruited to the distal D-box binding site. Even though UBE2S binds coactivator proteins[34,43] and generates Ub chains even in the absence of an E3 (ref. 44), we identified conditions in which APC/C stimulated UBE2S-mediated ubiquitination of UbcycB-NT* even in the absence of CDH1 (**Fig. 3b** and **Fig. 6a**). Although the K_i for full-length EMI1 increased substantially, presumably due to lack of its D-box recruitment by CDH1, the isolated EMI1^{T} inhibited APC/C–UBE2S–mediated ubiquitination of UbcycB-NT* equally well in the presence or absence of CDH1 (**Table 1** and **Fig. 6a**,**b**).

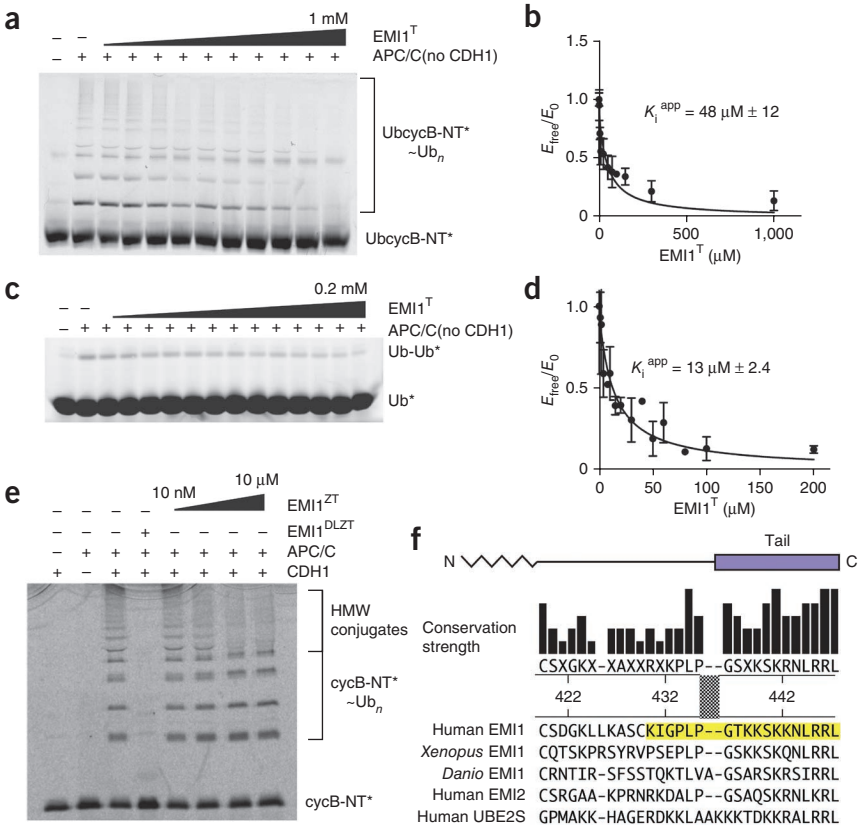

Figure 6 The EMI1 C-terminal tail is a specific inhibitor of APC/C- and UBE2S-dependent ubiquitin-chain formation. (**a**,**b**) Representative fluorescence scan of raw SDS-PAGE data (**a**) and curve fit (**b**) for inhibition of APC/C-dependent, CDH1-independent ubiquitination of UbcycB-NT* in the presence of increasing concentrations of a peptide corresponding to the EMI1 C-terminal tail ($EMI1^T$). Standard error of the mean (SEM), $n = 3$. (**c**,**d**) Representative fluorescence scan of raw SDS-PAGE data (**c**) and curve fit (**d**) for inhibition of APC/C-dependent, CDH1-independent ubiquitination of Ub* in the presence of increasing concentrations of a peptide corresponding to $EMI1^T$. SEM, $n = 3$. (**e**) Fluorescence detection of cycB-NT* ubiquitination by APC/C^{CDH1} by UBCH10 and UBE2S in the absence or presence of $EMI1^{DLZT}$ or increasing amounts of $EMI1^{ZT}$. $EMI1^{ZT}$ selectively inhibits formation of HMW conjugates formed when UBE2S is included in the reaction. (**f**) Alignment of EMI1 C-terminal sequences from the indicated organisms and the corresponding region of human EMI2 and UBE2S. Yellow highlight is the $EMI1^T$ peptide sequence.

The indifference to CDH1 implied that the isolated $EMI1^T$ targets a catalytic function of APC/C–UBE2S independently of blocking APC/C binding to a D-box substrate. We developed an assay for APC/C- and UBE2S-dependent synthesis of di-Ub chains, using as a substrate a Ub variant labeled with fluorescein on a C-terminal cysteine (**Fig. 6c**,**d**). Full-length EMI1 remained a superior inhibitor, with an order-of-magnitude lower K_i^{app} than that measured for $EMI1^{ZT}$ even for this substrate-independent Ub chain formation, suggesting that the structurally observed multisite APC/C binding enhances EMI1 inhibition of catalysis. Full-length EMI1 and $EMI1^{D(Mut)LZT}$ displayed similar degrees of inhibition, consistent with the notion that the D-box is recruited to CDH1. Inhibitory effects of $EMI1^{ZT}$, $EMI1^{Z}$ and $EMI1^{T}$ roughly paralleled those observed in CDH1-dependent ubiquitination of UbcycB-NT* (**Table 1**). Thus, $EMI1^T$ inhibits APC/C–UBE2S–catalyzed Ub-chain formation. Furthermore, this appears to be the case even in assays containing both UBE2S and UBCH10, as upon adding high concentrations of the shorter $EMI1^{ZT}$, we observed a selective decrease in the HMW products corresponding to those generated when UBE2S was included in the reactions (**Fig. 6e**). Comparing EMI1 and UBE2S sequences provides a rationale for the E2 selectivity, as the conserved residues in their C-terminal sequences are identical (**Fig. 6f**). Previous studies showed that the unique UBE2S C-terminal sequence is essential for APC/C recruitment[34,35].

DISCUSSION

At a global level, EMI1 shares some features with the other APC/C inhibitor, MCC. Both occupy the APC/C central cavity, on one end mimicking bound substrate and on the other binding and structurally reorganizing the platform to lock APC/C in a closed state (**Supplementary Fig. 8**)[5,45,46]. However, whereas the MCC is ~200 kDa and includes CDC20, APC/C is shut down by only a 143-residue C-terminal inhibitory domain from EMI1. Importantly, EMI1 is a distinct entity from CDH1, explaining how EMI1 can bind to APC/C already assembled with CDH1. Furthermore, between the EM data showing EMI1 contacting the APC/C catalytic core and biochemical data analyzing reactions inhibited by EMI1, we also uncovered a function for the unstructured C-terminal tail of EMI1 in blocking catalysis of Ub-chain elongation by UBE2S. As both EMI1 and UBE2S are found only in higher eukaryotes, this selective antagonism and the similar C-terminal sequences may reflect more recent evolution to bind a common site on APC/C from higher organisms.

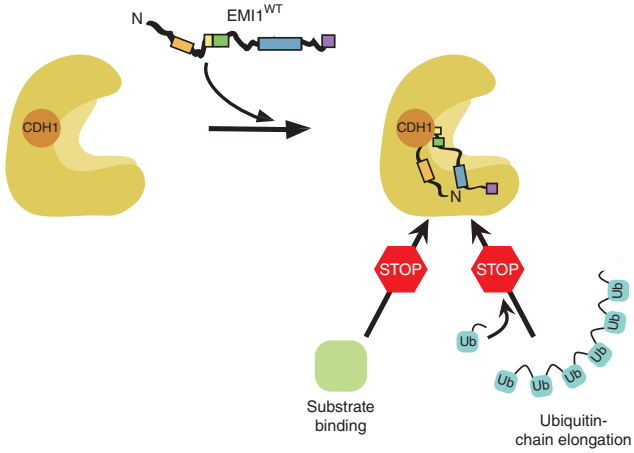

Figure 7 Mechanisms of APC/C inhibition model for EMI1 inhibition of APC/C^{CDH1}. EMI1's inhibitory C-terminal domain binds multiple sites for multimodal inhibition of APC/C^{CDH1}, blocking both substrate access to the D-box co-receptors CDH1 and APC10 and preventing Ub-chain elongation by UBE2S. The N-terminal domain of EMI1 is exposed, enabling regulation by binding to other partner proteins that modulate localization[18], EMI1 stability[14,20] and EMI1's ability to bind APC/C[49].

Alternatively, a key EMI1 function may be to block Ub-chain elongation. UBE2S is apparently required for normal mitosis only in a subset of cell types but in other cells may be important for recovery from the spindle checkpoint[33,34]. UBE2S-mediated Ub-chain elongation is thought to be particularly important for substrates with few lysines serving as sites of initial Ub ligation and may also be important for substrates whose turnover is regulated by deubiquitinating enzymes[32]. Thus, by extension, such substrates might also be especially sensitive to regulation by EMI1.

Notably, we found that EMI1's APC/C inhibitory domain is substantially natively disordered, thus defining a distinct structural class of E3 inhibitor and differing not only from the crystallographically characterized MCC but also from several other RING E3 inhibitors[2,3,9]. Intrinsic disorder enables a small sequence to have multiple discrete interaction motifs that mediate binding to multiple sites[47]. Consistent with prior studies, we detected inhibition by isolated D-box and EMI1 C-terminal tail peptides[23,48]. Our data also indicate that the linker and ZBR do not simply serve as spacers between the EMI1 D-box and C-terminal tail. We defined, for the first time, the linker as an effector of EMI1 function and identified surfaces on the linker and ZBR important for inhibiting APC/C. Each element is weak on its own, and the combination of the multiple motifs is required for maximal inhibition (**Fig. 7**).

The structural data provide a rationale for many previously described features of EMI1 regulation. In addition to inhibition by the C-terminal domain[22,23], EMI1 also plays a role in localizing a fraction of APC/C to spindle poles[18]. EM structures reveal that EMI1's N-terminal domain, which binds NuMA–dynein–dynactin to mediate localization, is exposed on the surface and available for interaction without disrupting contacts anchoring the C-terminal domain to APC/C^{CDH1} (**Supplementary Fig. 2d**). Ultimately, cell-cycle progression requires APC/C's liberation from EMI1. The exterior location of EMI1's N-terminal domain also explains how this region can be phosphorylated and ubiquitinated to signal EMI1 degradation before nuclear envelope breakdown[14,20]. Human EMI1's C-terminal domain is also blocked from APC/C binding through mitotic cyclin-dependent kinase–mediated phosphorylation[49]. These sites map to the EMI1 D-box and to within 5 Å of a bound zinc and the ZBR surface we identified as required for inhibition (**Fig. 5f**). It seems likely that EMI1's multisite binding to APC/C would enable the individual elements to fluctuate on and off, which would allow phosphorylation, in turn diminishing capacity for their rebinding and ultimately leading to separation from APC/C.

Although mechanisms by which intrinsic disorder can modulate protein function are only beginning to emerge, it is likely that many small, substantially intrinsically disordered domains utilize several elements to dynamically regulate multiple functionalities of massive molecular machines many times their size. As 30% of the human proteome is estimated to be natively unstructured[25], we anticipate that future studies will reveal other forms of E3-ligase regulation that depend on specialized features established by protein disorder.

METHODS

Methods and any associated references are available in the online version of the paper.

Accession codes. APC/C^{CDH1}–EMI1–SKP1, EMD-2354; APC/C^{CDH1}–EMI1^{DLZT}, EMD-2353; EMI1^{ZT}, 2M6N.

Note: Supplementary information is available in the online version of the paper.

ACKNOWLEDGMENTS

We are grateful to C.-G. Park, D. King, R. Pappu, B. Dye, C. Rock, P. Rodrigues and R. Cassell for advice and/or assistance. N.G.B. is a fellow of the Jane Coffin Childs Memorial Fund for Medical Research. The laboratory of R.W.K. was supported by American Lebanese Syrian Associated Charities (ALSAC), US National Institutes of Health (NIH) P30CA021765, R01CA082491 and 1R01GM08315. The laboratory of H.S. was supported by Deutsche Forschungsgemeinschaft Sonderforschungsbereich 860. The laboratory of J.-M.P. was supported by Boehringer Ingelheim, the Austrian Science Fund (FWF special research program SFB F34 'Chromosome Dynamics', grant W1221 'DK: Structure and Interaction of Biological Macromolecules' and Wittgenstein award Z196-B20), the Austrian Research Promotion Agency (FFG, Laura Bassi Center for Optimized Structural Studies), the Vienna Science and Technology Fund (WWTF LS09-13) and the European Community's Seventh Framework Programme (FP7/2007-2013) under grant agreement no. 241548 (MitoSys). The laboratory of B.A.S. was supported by ALSAC, NIH P30CA021765, R01GM065930 and the Howard Hughes Medical Institute. B.A.S. is an HHMI investigator.

AUTHOR CONTRIBUTIONS

J.-M.P., H.S. and B.A.S. planned and supervised the project. J.J.F., N.G.B., G.P., E.R.W., C.R.R.G., A.N. and M.A.J. designed the experiments. G.P. prepared samples for and contributed to EM experiments. J.J.F., N.G.B. and E.R.W. performed biochemical and biophysical analyses. A.N. performed analytical ultracentrifugation. C.R.R.G. and R.W.K. performed NMR analyses. H.S. performed EM. J.J.F., N.G.B., E.R.W., H.S. and B.A.S. prepared the manuscript with input from all authors.

COMPETING FINANCIAL INTERESTS

The authors declare no competing financial interests.

1. Deshaies, R.J. & Joazeiro, C.A. RING domain E3 ubiquitin ligases. *Annu. Rev. Biochem.* **78**, 399–434 (2009).
2. Barford, D. Structural insights into anaphase-promoting complex function and mechanism. *Phil. Trans. R. Soc. Lond. B* **366**, 3605–3624 (2011).
3. McLean, J.R., Chaix, D., Ohi, M.D. & Gould, K.L. State of the APC/C: organization, function, and structure. *Crit. Rev. Biochem. Mol. Biol.* **46**, 118–136 (2011).
4. da Fonseca, P.C. *et al.* Structures of APC/C(Cdh1) with substrates identify Cdh1 and Apc10 as the D-box co-receptor. *Nature* **470**, 274–278 (2011).
5. Chao, W.C., Kulkarni, K., Zhang, Z., Kong, E.H. & Barford, D. Structure of the mitotic checkpoint complex. *Nature* **484**, 208–213 (2012).
6. Buschhorn, B.A. *et al.* Substrate binding on the APC/C occurs between the coactivator Cdh1 and the processivity factor Doc1. *Nat. Struct. Mol. Biol.* **18**, 6–13 (2011).
7. Tian, W. *et al.* Structural analysis of human Cdc20 supports multisite degron recognition by APC/C. *Proc. Natl. Acad. Sci. USA* **109**, 18419–18424 (2012).
8. Musacchio, A. Spindle assembly checkpoint: the third decade. *Phil. Trans. R. Soc. Lond. B* **366**, 3595–3604 (2011).
9. Kim, S. & Yu, H. Mutual regulation between the spindle checkpoint and APC/C. *Semin. Cell Dev. Biol.* **22**, 551–558 (2011).
10. Herzog, F. *et al.* Structure of the anaphase-promoting complex/cyclosome interacting with a mitotic checkpoint complex. *Science* **323**, 1477–1481 (2009).
11. Dong, X. *et al.* Control of G1 in the developing *Drosophila* eye: rca1 regulates Cyclin A. *Genes Dev.* **11**, 94–105 (1997).
12. Reimann, J.D., Gardner, B.E., Margottin-Goguet, F. & Jackson, P.K. Emi1 regulates the anaphase-promoting complex by a different mechanism than Mad2 proteins. *Genes Dev.* **15**, 3278–3285 (2001).
13. Hsu, J.Y., Reimann, J.D., Sorensen, C.S., Lukas, J. & Jackson, P.K. E2F-dependent accumulation of hEmi1 regulates S phase entry by inhibiting APC(Cdh1). *Nat. Cell Biol.* **4**, 358–366 (2002).
14. Margottin-Goguet, F. *et al.* Prophase destruction of Emi1 by the SCF(betaTrCP/Slimb) ubiquitin ligase activates the anaphase promoting complex to allow progression beyond prometaphase. *Dev. Cell* **4**, 813–826 (2003).
15. Grosskortenhaus, R. & Sprenger, F. Rca1 inhibits APC-Cdh1(Fzr) and is required to prevent cyclin degradation in G2. *Dev. Cell* **2**, 29–40 (2002).
16. Di Fiore, B. & Pines, J. Emi1 is needed to couple DNA replication with mitosis but does not regulate activation of the mitotic APC/C. *J. Cell Biol.* **177**, 425–437 (2007).
17. Machida, Y.J. & Dutta, A. The APC/C inhibitor, Emi1, is essential for prevention of rereplication. *Genes Dev.* **21**, 184–194 (2007).
18. Ban, K.H. *et al.* The END network couples spindle pole assembly to inhibition of the anaphase-promoting complex/cyclosome in early mitosis. *Dev. Cell* **13**, 29–42 (2007).
19. Reimann, J.D. *et al.* Emi1 is a mitotic regulator that interacts with Cdc20 and inhibits the anaphase promoting complex. *Cell* **105**, 645–655 (2001).
20. Guardavaccaro, D. *et al.* Control of meiotic and mitotic progression by the F box protein beta-Trcp1 *in vivo*. *Dev. Cell* **4**, 799–812 (2003).

21. Hansen, D.V., Loktev, A.V., Ban, K.H. & Jackson, P.K. Plk1 regulates activation of the anaphase promoting complex by phosphorylating and triggering SCFbetaTrCP-dependent destruction of the APC Inhibitor Emi1. *Mol. Biol. Cell* **15**, 5623–5634 (2004).
22. Miller, J.J. *et al.* Emi1 stably binds and inhibits the anaphase-promoting complex/cyclosome as a pseudosubstrate inhibitor. *Genes Dev.* **20**, 2410–2420 (2006).
23. Ohe, M. *et al.* Emi2 inhibition of the anaphase-promoting complex/cyclosome absolutely requires Emi2 binding via the C-terminal RL tail. *Mol. Biol. Cell* **21**, 905–913 (2010).
24. Tang, W. *et al.* Emi2-mediated inhibition of E2-substrate ubiquitin transfer by the anaphase-promoting complex/cyclosome through a D-box-independent mechanism. *Mol. Biol. Cell* **21**, 2589–2597 (2010).
25. Dunker, A.K. *et al.* Intrinsically disordered protein. *J. Mol. Graph. Model.* **19**, 26–59 (2001).
26. Gieffers, C., Dube, P., Harris, J.R., Stark, H. & Peters, J.M. Three-dimensional structure of the anaphase-promoting complex. *Mol. Cell* **7**, 907–913 (2001).
27. Dube, P. *et al.* Localization of the coactivator Cdh1 and the cullin subunit Apc2 in a cryo-electron microscopy model of vertebrate APC/C. *Mol. Cell* **20**, 867–879 (2005).
28. Rodrigo-Brenni, M.C. & Morgan, D.O. Sequential E2s drive polyubiquitin chain assembly on APC targets. *Cell* **130**, 127–139 (2007).
29. Aristarkhov, A. *et al.* E2-C, a cyclin-selective ubiquitin carrier protein required for the destruction of mitotic cyclins. *Proc. Natl. Acad. Sci. USA* **93**, 4294–4299 (1996).
30. Yu, H., King, R.W., Peters, J.M. & Kirschner, M.W. Identification of a novel ubiquitin-conjugating enzyme involved in mitotic cyclin degradation. *Curr. Biol.* **6**, 455–466 (1996).
31. Summers, M.K., Pan, B., Mukhyala, K. & Jackson, P.K. The unique N terminus of the UbcH10 E2 enzyme controls the threshold for APC activation and enhances checkpoint regulation of the APC. *Mol. Cell* **31**, 544–556 (2008).
32. Dimova, N.V. *et al.* APC/C-mediated multiple monoubiquitylation provides an alternative degradation signal for cyclin B1. *Nat. Cell Biol.* **14**, 168–176 (2012).
33. Garnett, M.J. *et al.* UBE2S elongates ubiquitin chains on APC/C substrates to promote mitotic exit. *Nat. Cell Biol.* **11**, 1363–1369 (2009).
34. Williamson, A. *et al.* Identification of a physiological E2 module for the human anaphase-promoting complex. *Proc. Natl. Acad. Sci. USA* **106**, 18213–18218 (2009).
35. Wu, T. *et al.* UBE2S drives elongation of K11-linked ubiquitin chains by the anaphase-promoting complex. *Proc. Natl. Acad. Sci. USA* **107**, 1355–1360 (2010).
36. Meyer, H.J. & Rape, M. Processive ubiquitin chain formation by the anaphase-promoting complex. *Semin. Cell Dev. Biol.* **22**, 544–550 (2011).
37. Uzunova, K. *et al.* APC15 mediates CDC20 autoubiquitylation by APC/C(MCC) and disassembly of the mitotic checkpoint complex. *Nat. Struct. Mol. Biol.* **19**, 1116–1123 (2012).
38. Zeng, X. & King, R.W. An APC/C inhibitor stabilizes cyclin B1 by prematurely terminating ubiquitination. *Nat. Chem. Biol.* **8**, 383–392 (2012).
39. Carroll, C.W. & Morgan, D.O. The Doc1 subunit is a processivity factor for the anaphase-promoting complex. *Nat. Cell Biol.* **4**, 880–887 (2002).
40. Morrison, J.F. Kinetics of the reversible inhibition of enzyme-catalysed reactions by tight-binding inhibitors. *Biochim. Biophys. Acta* **185**, 269–286 (1969).
41. Burton, J.L. & Solomon, M.J. D box and KEN box motifs in budding yeast Hsl1p are required for APC-mediated degradation and direct binding to Cdc20p and Cdh1p. *Genes Dev.* **15**, 2381–2395 (2001).
42. Pashkova, N. *et al.* WD40 repeat propellers define a ubiquitin-binding domain that regulates turnover of F box proteins. *Mol. Cell* **40**, 433–443 (2010).
43. Wickliffe, K.E., Lorenz, S., Wemmer, D.E., Kuriyan, J. & Rape, M. The mechanism of linkage-specific ubiquitin chain elongation by a single-subunit E2. *Cell* **144**, 769–781 (2011).
44. Baboshina, O.V. & Haas, A.L. Novel multiubiquitin chain linkages catalyzed by the conjugating enzymes E2EPF and RAD6 are recognized by 26 S proteasome subunit 5. *J. Biol. Chem.* **271**, 2823–2831 (1996).
45. Sironi, L. *et al.* Crystal structure of the tetrameric Mad1-Mad2 core complex: implications of a 'safety belt' binding mechanism for the spindle checkpoint. *EMBO J.* **21**, 2496–2506 (2002).
46. Luo, X., Tang, Z., Rizo, J. & Yu, H. The Mad2 spindle checkpoint protein undergoes similar major conformational changes upon binding to either Mad1 or Cdc20. *Mol. Cell* **9**, 59–71 (2002).
47. Dyson, H.J. & Wright, P.E. Intrinsically unstructured proteins and their functions. *Nat. Rev. Mol. Cell Biol.* **6**, 197–208 (2005).
48. Reimann, J.D. & Jackson, P.K. Emi1 is required for cytostatic factor arrest in vertebrate eggs. *Nature* **416**, 850–854 (2002).
49. Moshe, Y., Bar-On, O., Ganoth, D. & Hershko, A. Regulation of the action of early mitotic inhibitor 1 on the anaphase-promoting complex/cyclosome by cyclin-dependent kinases. *J. Biol. Chem.* **286**, 16647–16657 (2011).
50. Kjaergaard, M. & Poulsen, F.M. Sequence correction of random coil chemical shifts: correlation between neighbor correction factors and changes in the Ramachandran distribution. *J. Biomol. NMR* **50**, 157–165 (2011).

ONLINE METHODS

Protein purification. EMI1 variants correspond to: EMI1^{NFDL}, residues 1–363; EMI1^{FDLZT}, residues 236–447; EMI1^{DLZT}, residues 305–447; EMI1^{ZT}, residues 363–447; EMI1^{NFDLZ}, residues 1–432. EMI1, ubiquitin variants, cycB-NT* and UbcycB-NT* were expressed as GST fusions, either from pGEX4T1 or pFastbac-GST modified to contain a TEV proteolytic site, and were purified by glutathione affinity chromatography, followed by His-TEV treatment. EMI1 and EMI1^{NFDL} were expressed in High Five cells. All other EMI1 variants were expressed in *Escherichia coli* BL21-Gold cells. All EMI1 variants containing an F-box were co-purified with SKP1. EMI1 wild-type and its variants were purified by ion exchange chromatography before sizing. GST-cycB-NT* and UbcycB-NT* were expressed in High Five cells treated with His-TEV, with GST and His-TEV removal by glutathione and nickel affinity chromatography. After sizing, cycB-NT* and UbcycB-NT* were FlAsH labeled using a C-terminal tetra-cysteine site. Other proteins were described previously[37].

APC/C^{CDH1}–EMI1 purification for electron microscopy. HeLa cells were grown in DMEM including 10% FBS (Invitrogen), 2 mM L-glutamine and 100 μg ml^{-1} penicillin/streptomycin (both from Sigma) and plated on 245 × 245–cm tissue culture dishes (NUNC). Cell extracts were prepared by lysis of frozen log-phase HeLa cells in extract buffer (20 mM Tris-HCl, pH 7.5, 150 mM NaCl, 2 mM EDTA, 10% (v/v) glycerol, 0.1% (w/v) octyl-β-D-glucopyranoside) using a Dounce homogenizer followed by centrifugation. APC/C was immunoprecipitated from the soluble fraction by incubation with an APC3 polyclonal peptide antibody (produced in rabbit) cross-linked to Affi-prep protein A beads from Bio-Rad at 1.33 μg per 1 μl beads[39]. Beads were washed four times (20 mM Tris-HCl, pH 7.5, 150 mM NaCl, 10% (v/v) glycerol, 0.1% (v/v) octyl-β-D-glucopyranoside), and the APC/C^{CDH1}–EMI1 complexes were reconstituted *in vitro* by mixing 3.5 μM PreScission-cleaved CDH1 and 150 nM EMI1–SKP1 with APC/C-bound APC3 antibody beads in binding buffer (20 mM Tris-HCl, pH 7.5, 150 mM NaCl, 0.1% (v/v) octyl-β-D-glucopyranoside, 4 mg ml^{-1} BSA. After a 1-h incubation, the beads were washed four times, and APC/C complexes were recovered by elution with antigenic peptides. APC/C^{CDH1_Flag}EMI1 complexes were enriched by re-immunoprecipitation experiments using anti-Flag M2 Agarose (Sigma) and subsequent elution with antigenic peptides. APC/C specimens were subjected to GraFix to further purify and stabilize the complexes.

Electron microscopy. Purified APC/C^{CDH1}–EMI1 complexes were adsorbed to a thin film of carbon and then transferred to an electron microscopic grid covered with a perforated carbon film. The bound APC/C particles were stained with 2% (w/v) uranyl formate, blotted and air-dried for ~1 min at room temperature. Images were recorded at a magnification of 119,000× or 155,000× on a 4k × 4k CCD camera (TVIPS GmbH) using two-fold pixel binning (2.5 Å or 1.8 Å per pixel) in a Philips CM200 FEG electron microscope (Philips/FEI) operated at 160 kV acceleration voltage. APC/C^{CDH1}–EMI1 complexes were analyzed as described[10].

Generation of recombinant human APC/C. Recombinant human APC/C was purified as described, using a C-terminal 2×-Strep tag on APC6 and an N-terminal GST tag on APC4 with the following modifications[37]. MultiBacs were constructed using donor plasmids pFL, pIDC, pIDK and pIDS[51], except the p10 baculoviral promoter was replaced with the polyhedron promoter and an additional polyadenylation site (SV40). Three MultiBacs were generated by Cre recombination of (i) pIDS CDC26/APC6-2xStrep-tagII, pFL APC11/APC2, pIDK APC10/APC5 and pIDC APC16/APC13; (ii) pIDC APC15/APC7 and pIDK APC8; and (iii) pFb APC1 with a loxP site from pIDC and pIDS APC3. GST-APC4 was expressed from a separate virus.

Enzyme assays. Proteins were purified in 20 mM Tris pH 7.6, 150 mM NaCl, 1 mM DTT. Ubiquitination assays were performed by combining two independent mixtures. One contained APC/C, 5 mM $MgCl_2$, 5 mM ATP, 0.25 mg mL^{-1} BSA, 1 μM CDH1, EMI1 and 100 nM UBA1. APC/C was incubated with CDH1 on ice for at least 30 min. Where included, EMI1 was added for 1 h to form APC/C^{CDH1}–EMI1 complexes. The second mixture contained E2, 125 μM bovine ubiquitin (Sigma) and substrate. Both mixtures were made on ice and equilibrated to room temperature before mixing. This combination prevents E2 autoubiquitination and allows the APC/C^{CDH1}–EMI1 complex to bind without competition by either E2 or substrate.

To determine the ½V_{max} CDH1 concentration and the K_m^{app} values for the E2s and substrates, the reactions were followed over time and the product bands were quantitated based on the FlAsH label on cycB-NT* or UbcycB-NT* or on fluorescein on Ub* using a PhosphorImager (Typhoon 9200) to determine the initial velocities. For CDH1-dependent reactions, CDH1-independent products were subtracted as background. For APC-dependent CDH1-independent reactions, APC/C-independent products were subtracted as background. To determine the K_i^{app} of wild-type EMI1 and variants, assay conditions that satisfy the requirements to be in the initial velocity were used so that a single time point could be used to determine the enzyme's initial velocity at each EMI1 concentration. Thus, to determine the K_i^{app} values of the EMI1 variants, concentrations of 5 nM APC/C, 900 nM UBCH10, 600 nM UBE2S, 120 nM cycB-NT* and 120 nM UbcycB-NT* were used. Reactions with the substrate cycB-NT* and UBCH10 were performed for 4 min, with the substrate UbcycB-NT* and the E2 UBCH10 for 4 min and with the substrate UbcycB-NT* and the E2 UBE2S for 2.5 min. The ½V_{max} and K_m values were determined by fitting the initial velocities to a hyperbolic curve/Michaelis-Menten, $v = V_{max}[X]/(K_m + [X])$, equation, where X is either the CDH1, UBCH10, UBE2S or substrate concentration.

Due to the tight binding nature of EMI1, K_i^{app} values were determined by method of Morrison[40]. The Morrison quadratic function accounts for both the depletion of enzyme and inhibitor. K_i^{app} values were determined by fitting the initial velocities to the Morrison tight binding equation (equation (1) using GraphPad Prism 6 software),

$$E_{free} = [E_0] - \frac{[E_0] + [I_0] + K_i^{app} - \sqrt{([E_0] + [I_0] + K_i^{app})^2 - (4[E_0][I_0])}}{2} \quad (1)$$

where E_{free} is the concentration of free enzyme determined by the residual APC/C^{CDH1} activity against the activity and concentration of the uninhibited APC/C^{CDH1} activity, $[E_0]$ is the total enzyme concentration and $[I_0]$ is the total inhibitor concentration. Simulations of theoretical K_i^{app} curves provided us with an upper limit of 2.5 nM for K_i^{app} values for the tight-binding versions of EMI1 (**Supplementary Fig. 5d**).

The CDH1, D-box substrate–independent Ub-chain formation assays were performed in the same conditions except the acceptor substrate was Ub fluorescein (Ub*) G75S-G76S-C77 with an additional C-terminal cysteine that prevents its utilization as a Ub donor. Experiments with APC/C in the absence of CDH1, with either UbcycB-NT* or Ub* as the substrates, were performed with UBE2S for 10 min.

Qualitative assays probing function of ZBR (30 nM EMI1) and linker (30 nM EMI1 in **Fig. 4**; 300 nM and 1 μM in **Supplementary Fig. 6**) were performed as described above except with concentrations of 13 nM APC/C, 10 nM UBA1, 190 nM UBCH10, 190 nM UBE2s, 20 nM cycB-NT* or 50 nM UbcycB-NT*. These reactions were quenched at 12 min.

NMR. *NMR spectroscopy.* NMR experiments were measured on either a Bruker 600 or 800 MHz spectrometer equipped with a ^{1}H and ^{13}C detect, TCI triple-resonance cryogenic probe using standard Bruker pulse programs. ^{15}N-^{1}H HSQC spectra were collected at 25 °C. ^{1}H, ^{13}C and ^{15}N backbone resonances were assigned using standard triple-resonance experiments, such as HNCA, HNCACB and CBCA(CO)NH. The side-chain ^{1}H resonances were assigned using (H)CCH-TOCSY and H(CCCO)NH experiments. Aromatic side-chain assignments were obtained with two-dimensional [^{13}C, ^{1}H]-HSQC and three-dimensional ^{13}C-resolved aromatic [^{1}H, ^{1}H]-NOESY experiments. Distance constraints for the structure calculation were derived from three-dimensional ^{13}C-aliphatic, ^{13}C-aromatic and ^{15}N-resolved [^{1}H, ^{1}H]-NOESY spectra recorded with a mixing time of 100 ms. ^{1}H chemical shifts were referenced with respect to DSS measured in the same buffer, whereas ^{13}C and ^{15}N chemical shifts were referenced indirectly with respect to the DSS shift. Spectra were processed using Topspin software and analyzed using the computer-aided resonance software CARA[52]. Heteronuclear ^{15}N {^{1}H} NOEs for EMI1^{DLZT} were measured using a 5 s irradiation period and 2 s relaxation delay (NOE) or a 7 s relaxation delay (no NOE) on the ^{13}C, ^{15}N-labeled sample used for structure calculation.

NMR structure calculations. Structures were determined using a combination of manually assigned NOEs and automatic NOE assignment using the program CYANA[53]. Approximately 931 meaningful distance restraints, 38 angle restraints derived from CA and CB shifts using the program TALOS+[54], 8 zinc ion distances

doi:10.1038/nsmb.2593

and 32 hydrogen bond restraints based on exchange cross-peaks with water in the ^{15}N-NOESY spectrum were used in the structure calculation of EMI1^{ZT} (**Table 2**). Seven iterations of refinement for 100 structures per cycle were completed after proper distance calibrations. After the initial fold of the protein was determined, a CYANA amino acid library using a modified zinc-ligated cysteine residue was used to incorporate the two zinc ions into the structures.

Generation of metal-free EMI1^{ZT} and zinc reconstitution. ^{15}N-labeled EMI1^{ZT} was incubated in 10 mM sodium phosphate (pH 6.5), 50 mM NaCl, 1 mM DTT and 20 mM EDTA and then dialyzed against 10 mM sodium phosphate (pH 6.5), 50 mM NaCl, 1 mM DTT. Unfolding was confirmed by measuring one- and two-dimensional ^{1}H-^{15}N HSQC spectra post-dialysis. Six rounds of dialysis resulted in removal of EDTA. Dialysis against 10 mM sodium phosphate (pH 6.5), 50 mM NaCl, 1 mM DTT, 200 μM ZnSO4 restored zinc.

51. Bieniossek, C., Richmond, T.J. & Berger, I. MultiBac: multigene baculovirus-based eukaryotic protein complex production. *Curr. Protoc. Protein Sci.* **51**, 5.20 (2008).
52. Keller, R.L.J. The computer aided resonance assignment tutorial. ⟨http://cara.nmr-software.org/downloads/3-85600-112-3.pdf⟩ (CANTINA Verlag, Zurich, 2004).
53. Güntert, P., Mumenthaler, C. & Wuthrich, K. Torsion angle dynamics for NMR structure calculation with the new program DYANA. *J. Mol. Biol.* **273**, 283–298 (1997).
54. Shen, Y., Delaglio, F., Cornilescu, G. & Bax, A. TALOS+: a hybrid method for predicting protein backbone torsion angles from NMR chemical shifts. *J. Biomol. NMR* **44**, 213–223 (2009).